Quantification of the Structure of Colloidal Gas–Liquid Interfaces

Supporting Information

Mark Vis, Kelly J.H. Brouwer, Álvaro González García,
Andrei V. Petukhov, Oleg Konovalov, Remco Tuinier

September 18, 2020

1 Materials

Polydimethylsiloxane (PDMS) with a molar mass of $117\,\mathrm{kg\,mol^{-1}}$ was used (Alfa Aesar, no. 42504). For PDMS in cyclohexane, the radius of gyration R_g is approximately given by

$$R_g = 0.0149 M_w^{0.6}, \tag{S1}$$

with R_g in nm and M_w in $\mathrm{g\,mol^{-1}}$.[1–3] This yields $R_g \approx 16.4\,\mathrm{nm}$.

Ludox TMA silica nanoparticles (Sigma-Aldrich, no. 420859) were hydrophobized by reaction of the surface silanol-groups with stearyl-alcohol (1-octadecanol, Sigma-Aldrich, 95 %, no. O709) as described elsewhere in detail[4,5] and subsequently dispersed in cyclohexane (Biosolve, AR, no. 031305). Analysis with transmission electron microscopy of $N = 1766$ particles shows that the particles have an average diameter $d = 29.2 \pm 3.8\,\mathrm{nm}$ (Fig. S1a). Analysis of the form factor of the particles using small-angle X-ray scattering performed at beamline ID02 at the European Synchrotron Radiation Facility (ESRF) in Grenoble shows $d = 29.4 \pm 2.2\,\mathrm{nm}$, assuming a log-normal distribution in particle diameter (Fig. S1b).

The phase diagram in the main text was obtained by using the method of Bodnár and Oosterhuis [6].

2 X-ray reflectivity measurements

X-ray reflectivity measurements were carried out at the ESRF in Grenoble, on beamline ID10, endstation EH1 at a photon energy of 22 keV ($\lambda = 0.56\,\text{Å}$).[7] A 1D-detector (Mythen 1K) was placed horizontally (parallel to interface) under specular conditions, i.e., keeping

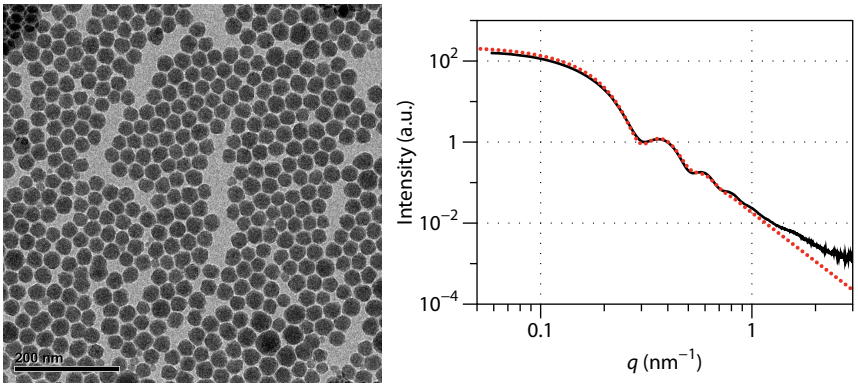

(a) **(b)**

Figure S1: (a) Transmission electron micrograph of the stearyl-coated silica colloids. (b) Small-angle X-ray scattering analysis of the form factor of a dilute particle dispersion in cyclohexane, where the solid black curve represents experimental data and the red dotted curve is a fit assuming a log-normal size distribution of the colloidal spheres.

the detector angle the same as the grazing angle, denoted as θ (see Fig. S2). A vertical slit size of 0.4 mm and a detector distance of about 85 cm were used, resulting in a selection angle of about 0.03°. The raw data was obtained by scanning the angle θ at least twice per sample.

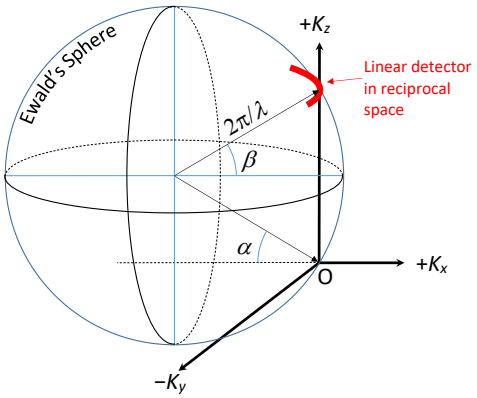

Figure S2: Schematic representation of the definitions of the scattering vectors K_x, K_y, and K_z for our X-ray reflectivity experiments. The grazing angle α equals the detector angle β and are collectively denoted as θ in this work.

Home-built aluminum sample cells with dimensions of $7.5 \times 1.0 \times 0.50\,\mathrm{cm}^3$ (L × H × W) were used, with the long axis parallel to the beam. The long ends of the sample cells were equipped with Kapton windows. Samples were mixed at the desired concentration in separate vials and, while stirring, transferred to the sample cell with a pipette, which were

subsequently closed to prevent evaporation of the solvent. Samples were equilibrated for several hours to several days until a stable X-ray reflectivity measurement was obtained. After equilibrium was reached, to the naked eye the samples appeared transparent and a sharp interface, visible under certain angles, separated the colloid-rich bottom phase from the colloid-poor top phase. We found it necessary to limit the intensity of the X-rays to prevent local heating effects from disturbing the interface. The results (averaged over multiple scans) are shown for all samples in Fig. S3.

As can be seen clearly in Fig. S3, the reflected beam 'sits' on a background caused by bulk scattering (form factor and structure factor) of colloidal particles. Since for small K_y (parallel to the interface) the Guinier approximation holds, this feature was used to correct for bulk scattering for each individual scan. It is therefore assumed that the logarithm of the background intensity due to scattering follows $\ln I_{\mathrm{bg}} = b - a(x - x_{\mathrm{center}})^2$, where x is the pixel position on the 1D detector (oriented along the K_y direction), x_{center} denotes the center position of reflected beam, and a and b are fit parameters. The fit parameters a and b are determined individually for each scan at each angle, whereas x_{center} is obtained through imaging the direct beam and set to the same value throughout. The background was assumed to be symmetrical and fitted to pixels $x - x_{\mathrm{center}} = -13$ to -4 and $+4$ to $+13$ simultaneously. The reflected beam, minus background, was subsequently integrated over a region of $x - x_{\mathrm{center}} = -3$ to $+3$. For each sample, the results of multiple scans were subsequently fitted individually and the obtained fit parameters averaged per sample. The effect of the background correction is illustrated in Fig. S4. It should be stressed that this background correction does not modify the slope after the critical angle, but merely makes this slope visible over a larger K_z-range, and therefore facilitates the fitting process.

In analyzing the experimental data, the parameters listed in Table S1 were assumed. For simplicity, it was assumed that the difference in refractive index of the two coexisting phases was dominated by cyclohexane and silica, and that the PDMS had a negligible contribution. We assumed volume fraction-weighted refractive indices. For simplicity, the refractive index of the colloid-poor top phase n_{t} is fixed to the value of cyclohexane. The refractive index of the colloid-rich bottom phase n_{b} follows from $\delta_{\mathrm{b}} = \Delta\phi\delta_{\mathrm{silica}} + (1 - \Delta\phi)\delta_{\mathrm{cyclohexane}}$ and $\beta_{\mathrm{b}} = \Delta\phi\beta_{\mathrm{silica}} + (1 - \Delta\phi)\beta_{\mathrm{cyclohexane}}$. The colloid volume fraction difference $\Delta\phi$ and the interfacial width σ are determined through a least-squares fit of $\log R(\theta)$. The resulting fit parameters, averaged per sample, are shown in Table S2.

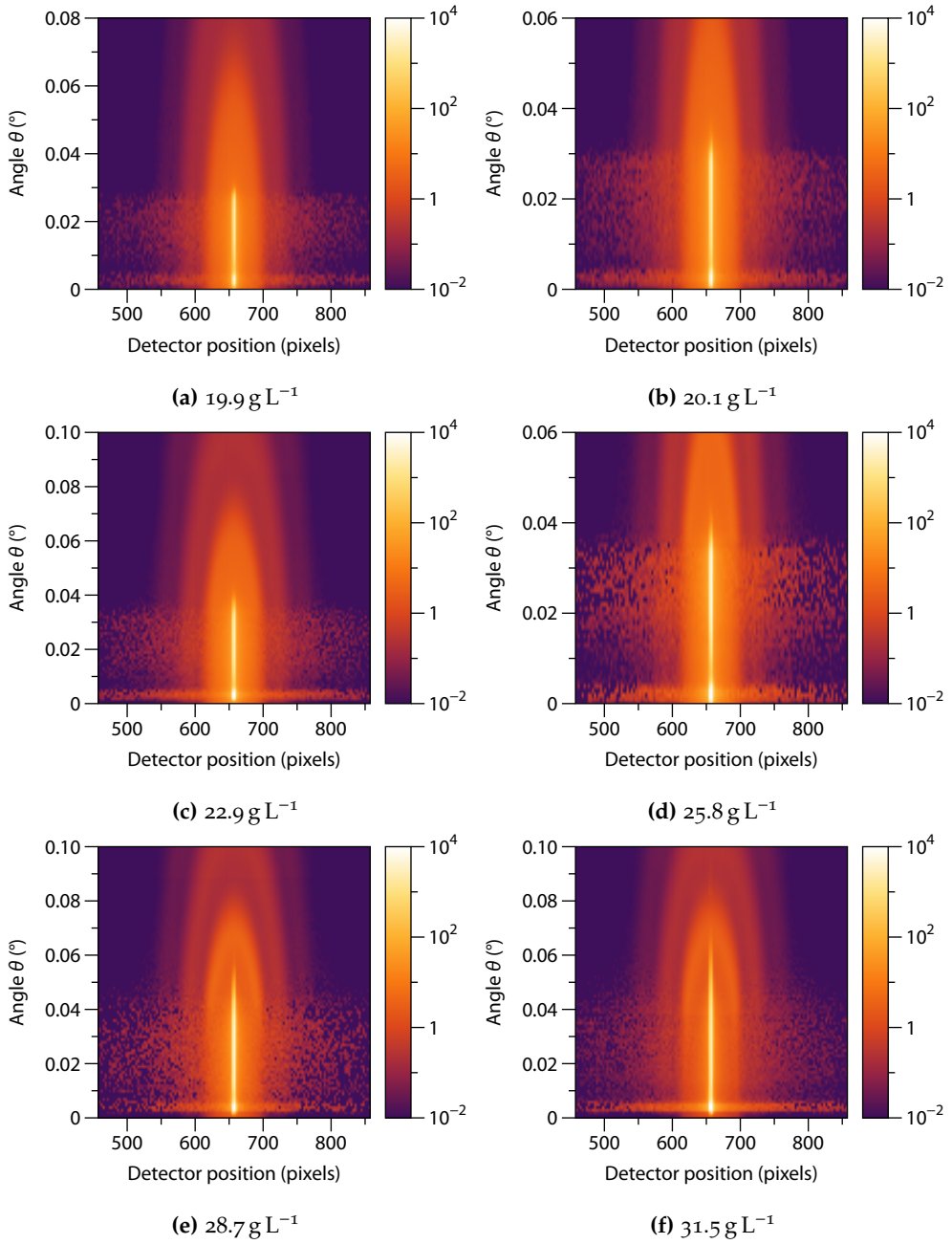

(a) 19.9 g L^{-1} **(b)** 20.1 g L^{-1}

(c) 22.9 g L^{-1} **(d)** 25.8 g L^{-1}

(e) 28.7 g L^{-1} **(f)** 31.5 g L^{-1}

Figure S3: X-ray reflectivity density plots for colloidal gas–liquid interfaces in samples consisting of 141 g L^{-1} colloidal silica spheres ($d = 29.4 \pm 2.2$ nm) and non-adsorbing polymer (PDMS, 117 kDa, $R_g \approx 16.4$ nm) at the indicated concentration.

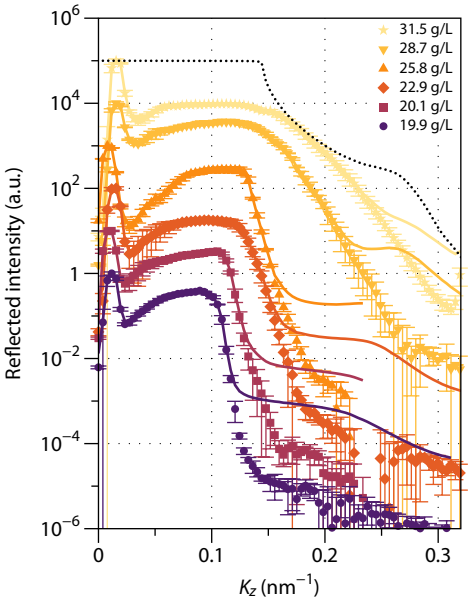

Figure S4: The effect of background subtraction on the experimental reflectivity data. The solid curves are the data before background correction, while the points are the data after background correction. Error bars indicate the standard deviation between multiple scans of the same sample (only shown for the corrected data for clarity). The curves are shifted vertically for legibility. The black dotted curve is the *calculated* reflectivity based on the oscillatory density profiles from the DFT-work of Brader et al.,[8] with $\Delta\phi \approx 0.44$ and $q = 0.6$ (see Figure 2a in their paper).

Table S1: Overview of the real (δ) and imaginary (β) components of the refractive indices for X-rays with an energy of 22 keV ($\lambda = 0.56$ Å)[9] and mass densities ρ[10] of the components assumed in this study.

	δ	β	ρ (g mL^{-1})
cyclohexane	3.81×10^{-7}	1.10×10^{-10}	0.779
silica	9.44×10^{-7}	1.75×10^{-9}	≈ 2.2

Table S2: Parameters of the fits of the reflectivity data in the main text for samples with polymer concentrations c_{polymer}.

	n_t		n_b			
c_{polymer} (g L^{-1})	δ_t	β_t	δ_b	β_b	$\Delta\phi$	σ (nm)
19.9	3.81×10^{-7}	1.10×10^{-10}	4.96×10^{-7}	4.47×10^{-10}	0.2053 ± 0.0023	28.3 ± 0.6
20.1	3.81×10^{-7}	1.10×10^{-10}	5.12×10^{-7}	4.91×10^{-10}	0.2321 ± 0.0023	22.3 ± 1.3
22.9	3.81×10^{-7}	1.10×10^{-10}	5.52×10^{-7}	6.10×10^{-10}	0.305 ± 0.010	19.4 ± 0.9
25.8	3.81×10^{-7}	1.10×10^{-10}	5.56×10^{-7}	6.20×10^{-10}	0.3107 ± 0.0012	19.4 ± 0.3
28.7	3.81×10^{-7}	1.10×10^{-10}	6.63×10^{-7}	9.32×10^{-10}	0.501 ± 0.008	12.4 ± 0.7
31.5	3.81×10^{-7}	1.10×10^{-10}	6.71×10^{-7}	9.56×10^{-10}	0.516 ± 0.029	10.50 ± 0.20

3 GFVT

In the theoretical description of the colloid–polymer mixtures, models comprising penetrable hard spheres (PHS), polymers in theta solvent conditions, and polymers in good solvent conditions were used. The free-volume fraction α is given by

$$\alpha(\phi_{\mathrm{d}}^{\mathrm{R}}) = (1-\phi)\exp(-Q_{\mathrm{S}})\exp(-q^{*3}\widetilde{\Pi}_0), \tag{S2}$$

with

$$Q_{\mathrm{S}} = 3yq^* + 0.5y(9y+6)q^{*2}, \tag{S3a}$$

$$y = \frac{\phi}{1-\phi}, \tag{S3b}$$

where q^* denotes the effective size of the depletion zones, and $\widetilde{\Pi}_0$ is the osmotic pressure of a polymer-free hard sphere fluid.

The relevant equations for the osmotic pressure and effective depletion zone size are given in the following for the various polymer descriptions. For PHS:

$$\widetilde{\Pi}_{\mathrm{d}}^{\mathrm{R}} = \phi_{\mathrm{d}}^{\mathrm{R}}, \tag{S4a}$$

$$q^* = q. \tag{S4b}$$

For theta solvent conditions:[11]

$$\widetilde{\Pi}_{\mathrm{d}}^{\mathrm{R}} = \phi_{\mathrm{d}}^{\mathrm{R}} + 4.1(\phi_{\mathrm{d}}^{\mathrm{R}})^3, \tag{S5a}$$

$$q^* = 0.938\left[\frac{q}{\sqrt{1+6.02(\phi_{\mathrm{d}}^{\mathrm{R}})^2}}\right]^{0.9}. \tag{S5b}$$

For polymers in good-solvent conditions,[11]

$$\widetilde{\Pi}_{\mathrm{d}}^{\mathrm{R}} = \phi_{\mathrm{d}}^{\mathrm{R}} + 1.61(\phi_{\mathrm{d}}^{\mathrm{R}})^{2.31}, \tag{S6a}$$

$$q^* = 0.865\left[\frac{q}{\sqrt{1+3.95(\phi_{\mathrm{d}}^{\mathrm{R}})^{1.54}}}\right]^{0.88}. \tag{S6b}$$

A phase diagram for these different polymer descriptions is given in Fig. S5.

The second moment of the direct correlation function $c(\widetilde{r})$ is given by

$$\widetilde{m} = \frac{\pi}{3}\int_0^\infty c(\widetilde{r})\widetilde{r}^4 \mathrm{d}\widetilde{r}. \tag{S7}$$

Here $\widetilde{r} \equiv r/d$ is the normalized center-to-center distance between two colloids. We use the mean-spherical approximation (MSA),[12] $c(\widetilde{r}) = -U(\widetilde{r})$ for $\widetilde{r} \geq 1$, which becomes accurate for long-ranged interactions. In general, the depletion pair potential $U(\widetilde{r})$ reads:

$$\frac{U(\widetilde{r})}{k_{\mathrm{B}}T} = -\int_0^{\phi_{\mathrm{d}}^{\mathrm{R}}} \mathrm{d}\phi_{\mathrm{d}}^{\mathrm{R}\prime}\left(\frac{\partial\widetilde{\Pi}_{\mathrm{d}}^{\mathrm{R}}}{\partial\phi_{\mathrm{d}}^{\mathrm{R}\prime}}\right)\frac{v_{\mathrm{overlap}}}{v_{\mathrm{d}}}, \tag{S8}$$

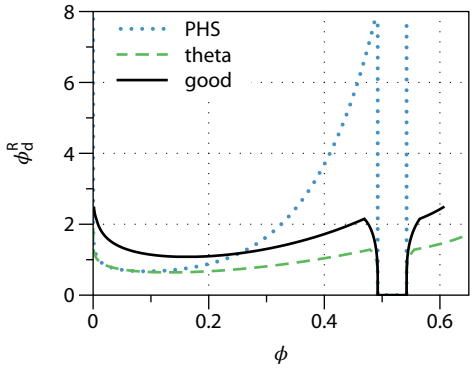

Figure S5: Phase diagram for $q = 1.1$ as calculated using GFVT.

where $v_d = 4\pi R_g^3/3$. The overlap volume $v_{overlap}$ of depletion zones of two colloids follows from geometric arguments

$$\frac{v_{overlap}}{v_d} = q^{-3}q^{*3}\left(\frac{1}{q^*}+1\right)^3\left[1-\frac{3\widetilde{r}}{2(q^*+1)}+\frac{\widetilde{r}^3}{2(q^*+1)^3}\right], \tag{S9}$$

for $1 \leq \widetilde{r} \leq 1+q^*$ (it is zero otherwise). The above means that, although generally $\widetilde{m}$ is a function of the colloid volume fraction ϕ,[13] here it is only a function of q and the polymer reservoir volume fraction ϕ_d^R for a given polymer model.

Some representative interfacial profiles for PHS and polymers in theta solvent are given in Fig. S6, profiles for polymers in good solvent are given in the main text. Overall the profiles fit reasonably well to a Gaussian description,

$$\phi(z) = \phi^g + \frac{1}{2}\Delta\phi\left[1+\mathrm{erf}\left(\frac{z}{\sqrt{2}\sigma}\right)\right], \tag{S10}$$

shown as the dashed curves, although some differences can be observed, notably for the PHS-case at large $\Delta\phi$. Other approaches to quantify the width also exist, such as the width ξ defined by a hyperbolic tangent

$$\phi(z) = \phi^g + \frac{1}{2}\Delta\phi\left[1+\tanh\left(\frac{z}{\xi}\right)\right], \tag{S11}$$

which provides fits of similar quality (not shown), or the "10–90% width" W_{10-90}.[14] A comparison of the widths obtained this way is given in Fig. S7a and Table S3, showing that these various definitions essentially only differ by a constant factor.

A comparison of the calculated interfacial tension for the various models is given in Fig. S7b, together with experimental results by Aarts *et al.*[15] for a similar system. Note that, in order to make a valid comparison with those experimental results, in this specific case the dimensionless interfacial tension $\widetilde{\gamma}$ as obtained from GFVT was converted into γ using the specific diameter of the particles of Aarts *et al.*, being $d = 26\,\mathrm{nm}$.

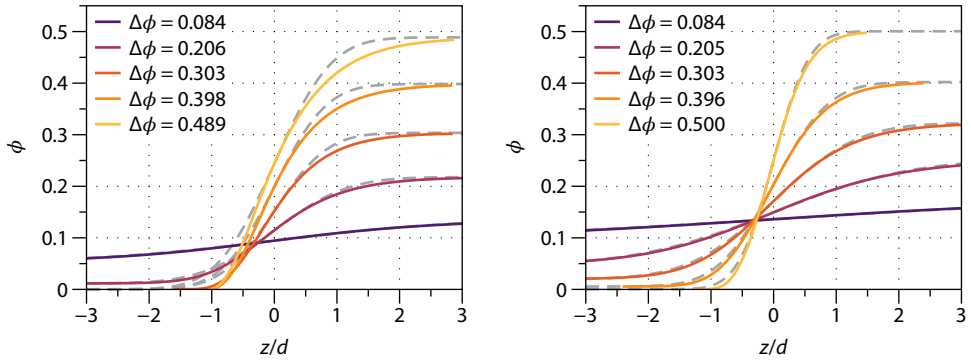

(a) penetrable hard spheres **(b)** polymers in theta solvent

Figure S6: Colloid density profiles (solid curves) as calculated using generalized free-volume theory for penetrable hard spheres and for polymers in a theta solvent, including corresponding Gaussian fits (dashed curves). The interfacial widths are $\sigma/d = 2.30, 0.92, 0.67, 0.66$, and 0.72 and $\sigma/d = 4.50, 1.72, 1.06, 0.70$, and 0.45, respectively, for the indicated values of the colloid density difference $\Delta\phi$ (top to bottom).

Table S3: Average ratio between the hyperbolic tangent width ξ and the Gaussian width σ, and the 10–90% width W_{10-90} and the Gaussian width σ, for the data shown in Fig. S7a.

	$\langle \xi/\sigma \rangle$	$\langle W_{10-90}/\sigma \rangle$
PHS	1.189 ± 0.008	2.65 ± 0.03
theta solvent	1.1780 ± 0.0010	2.582 ± 0.006
good solvent	1.1771 ± 0.0006	2.575 ± 0.007
overall	1.180 ± 0.006	2.59 ± 0.03

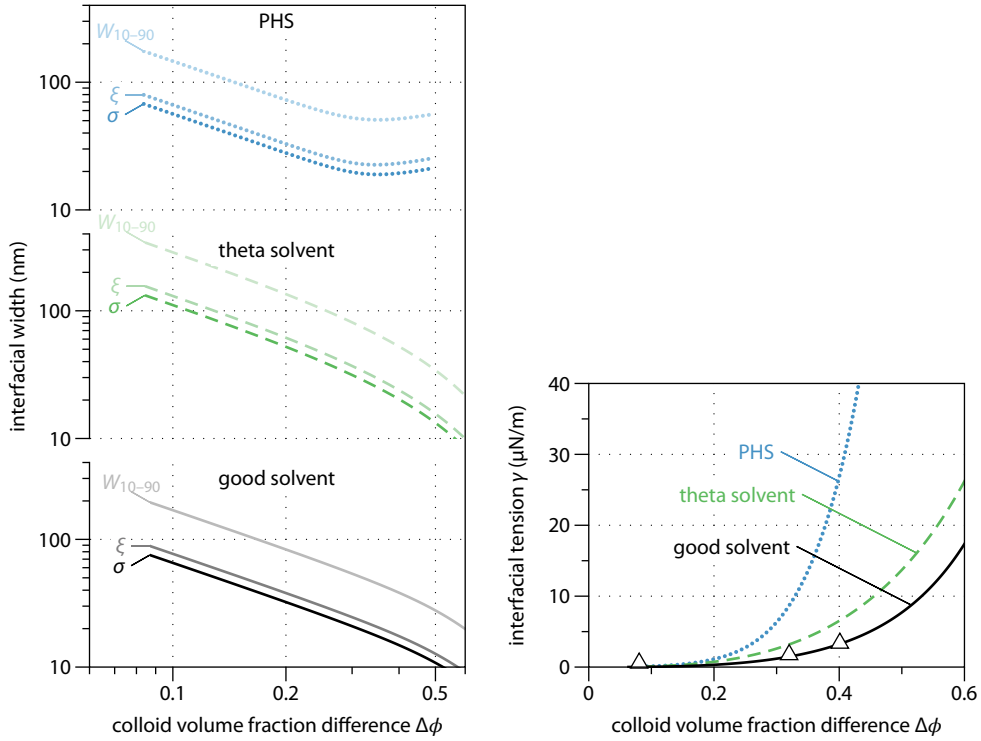

Figure S7: (a) The interfacial width as a function of the colloid gas–liquid density difference $\Delta\phi$ as calculated using (generalized) free-volume theory for (top) penetrable hard spheres, (middle) polymers in a theta solvent, and (bottom) polymers in a good solvent. Within each panel, the 10–90% width W_{10-90}, the hyperbolic tangent width ξ, and the Gaussian width σ are shown (top to bottom, light to dark curves, using $d = 29.4\,\text{nm}$ of our particles). (b) The interfacial tension resulting from (G)FVT, compared to experiments by Aarts *et al.* (open triangles, using $d = 26\,\text{nm}$).[15]

References

(1) Ouhajji, S.; Nylander, T.; Piculell, L.; Tuinier, R.; Linse, P.; Philipse, A. P. Depletion controlled surface deposition of uncharged colloidal spheres from stable bulk dispersions. *Soft Matter* **2016**, *12*, 3963–3971.

(2) Vincent, B. The calculation of depletion layer thickness as a function of bulk polymer concentration. *Colloids and Surfaces* **1990**, *50*, 241–249.

(3) Vincent, B.; Edwards, J.; Emmett, S.; Croot, R. Phase separation in dispersions of weakly-interacting particles in solutions of non-adsorbing polymer. *Colloids and Surfaces* **1988**, *31*, 267–298.

(4) Van Helden, A. K.; Jansen, J. W.; Vrij, A. Preparation and characterization of spherical monodisperse silica dispersions in nonaqueous solvents. *Journal of Colloid and Interface Science* **1981**, *81*, 354–368.

(5) Pathmamanoharan, C.; Philipse, A. P. Preparation of small alkane-grafted silica particles (for SAXS and SANS studies) from aqueous commercial sols. *Journal of Colloid and Interface Science* **1994**, *165*, 519–521.

(6) Bodnár, I.; Oosterbaan, W. D. Indirect determination of the composition of the coexisting phases in a demixed colloid polymer mixture. *The Journal of Chemical Physics* **1997**, *106*, 7777–7780.

(7) Smilgies, D.-M.; Boudet, N.; Struth, B.; Konovalov, O. Troika II: a versatile beamline for the study of liquid and solid interfaces. *Journal of Synchrotron Radiation* **2005**, *12*, 329–339.

(8) Brader, J. M.; Evans, R.; Schmidt, M. Entropic wetting and the fluid–fluid interface of a model colloid–polymer mixture. *Journal of Physics: Condensed Matter* **2002**, *14*, L1–L8.

(9) Henke, B. L.; Gullikson, E. M.; Davis, J. C. X-ray interactions: photoabsorption, scattering, transmission, and reflection at E= 50–30,000 eV, Z= 1–92. *Atomic data and nuclear data tables* **1993**, *54*, 181–342.

(10) *CRC Handbook of Chemistry and Physics*, 90th Edition; Lide, D. R., Ed.; CRC Press/Taylor and Francis: Boca Raton, FL, 2009.

(11) Fleer, G. J.; Tuinier, R. Analytical phase diagrams for colloids and non-adsorbing polymer. *Advances in Colloid and Interface Science* **2008**, *143*, 1–47.

(12) Aarts, D. G. A. L.; Dullens, R. P. A.; Lekkerkerker, H. N. W.; Bonn, D.; van Roij, R. Interfacial tension and wetting in colloid–polymer mixtures. *The Journal of Chemical Physics* **2004**, *120*, 1973–1980.

(13) Rowlinson, J. S.; Widom, B., *Molecular theory of capillarity*; Dover Publications: 1982.

(14) Brader, J. M.; Evans, R. The fluid–fluid interface of a model colloid–polymer mixture. *Europhysics Letters* **2000**, *49*, 678–684.

(15) Aarts, D. G. A. L.; van der Wiel, J. H.; Lekkerkerker, H. N. W. Interfacial dynamics and the static profile near a single wall in a model colloid–polymer mixture. *Journal of Physics: Condensed Matter* **2003**, *15*, S245–S250.